



Data description submitted to Earth System Science Data

A global dataset of the shape of drainage systems

Chuanqi He^{1,2,3}, Ci-Jian Yang⁴, Jens M. Turowski¹, Richard F. Ott^{1,5},
Jean Braun¹, Hui Tang¹, Shadi Ghantous⁶, Xiaoping Yuan³, Gaia Stucky de Quay²

5

¹German Research Centre for Geosciences, Potsdam

²Department of Earth, Atmospheric & Planetary Sciences, Massachusetts Institute of Technology, Cambridge

³School of Earth Sciences, China University of Geosciences, Wuhan

⁴Department of Geography, National Taiwan University, Taipei

⁵Institute for Biodiversity and Ecosystem Dynamics, University of Amsterdam, Amsterdam

10

⁶Institute of Environmental Science and Geography, University of Potsdam, Potsdam

Correspondence: Chuanqi He (chuanqi@gfz-potsdam.de)

Abstract. Drainage basins delineate the Earth's land surface into individual water collection units. Basin shape and river sinuosity determine water and sediment dynamics, affecting landscape evolution and connectivity between ecosystems and freshwater species. However, a high-resolution global dataset for the boundaries and geometry of basins is still missing. Using a 90-meter resolution digital elevation model, we measured the areas, lengths, widths, aspect ratios, slopes, and elevations for basins greater than 50 km² globally. Additionally, we calculated the lengths and sinuosities of the longest river channels within these 0.67 million basins. We built a new global dataset, Basin90m, to present the basins and rivers, as well as their morphological metrics. To highlight the use cases of Basin90m, we explored differences between the nine stream orders, spatial distribution of drainage systems, and correlations between morphological metrics, such as Hack's law. By comparing with HydroSHEDS, Google Earth images, and a few other datasets, we have demonstrated the high accuracy of Basin90m. Basin90m, available in Shapefile format, can be used in various GIS platforms, including QGIS, ArcGIS, and GeoPandas. Basin90m has substantial application prospects in geomorphology, hydrology, and ecology.

1 Introduction

The shape of drainage basins and rivers holds significant implications for landscape evolution processes and dynamics (Ielpi et al., 2023). With equal basin lengths, a broader basin delivers more water and sediments downstream. Similarly, given the same elevation drop, a meandering river has a milder channel gradient than a straight river and therefore may feature smaller erosion rates. Meanwhile, meandering rivers create a mosaic of habitats with varying flow velocities, depths, and substrates, supporting the diversity of aquatic organisms (Nagayama and Nakamura, 2017; Rhoads et al., 2003; Yu et al., 2022). Additionally, the shape of drainage systems is argued to be related to climatic and tectonic conditions (Castelltort et al., 2012; Ielpi et al., 2023; Luo et al., 2023; Sreedevi et al., 2009; Strong and Mudd, 2022), and could therefore be used as an archive. Accordingly, a global dataset on the shape of drainage systems benefits scientists and policymakers in geomorphology, hydrology, and ecology, fostering



40 interdisciplinary collaborations.

In the past three decades, digital elevation models (DEMs) have been utilized to produce several global-scale drainage basin and river databases (Allen and Pavelsky, 2018; Amatulli et al., 2022; Lin et al., 2021; Masutomi et al., 2009; Shen et al., 2017; Vörösmarty et al., 2000). Using 1-km resolution DEM, the U.S. Geological Survey (USGS) developed HYDRO1k
45 (USGS, 2000), a global hydrological dataset providing vector basin boundaries and river channels. HydroSHEDS (Lehner and Grill, 2013; Lehner et al., 2008) provides 500-m resolution global basins and rivers and their basic metrics, such as area, river length, and stream order. HydroSHEDS encompasses one million drainage basins. HydroSHEDS basin boundaries and a 500-m resolution DEM were utilized to calculate morphometric indices for 26272
50 drainage basins worldwide with an area larger than 100 km² (Guth, 2011). These indices include basin elevation and slope. HydroATLAS (Linke et al., 2019) was developed based on HydroSHEDS and incorporates 56 hydro-environmental attributes, including basin-mean slope and elevation.

Recently, with the advancements in computer performance and algorithms, the 90-m
55 resolution DEMs are being used to establish global databases of drainage systems. For example, USGS released HDMA, which has a resolution of 90 m (Verdin, 2017). It includes nearly 295000 drainage basins and contains area attributes. GRNWRZ (Yan et al., 2022) comprises a global river database at a resolution of 90 m, including information on the length of rivers. This database offers the boundaries and areas of water resource zones distinct from drainage basins.

60 In summary, drainage basins and rivers have been mapped, along with measurements of area, slope, and elevation of basins. Yet, few works have focused on more complex basin characteristics, such as aspect ratio, which describes the shape of drainage basins, and sinuosity that characterizes the shape of river channels. Here, we used a global 90-m resolution DEM and obtained over 665000 drainage basins with a size greater than 50 km². For each basin, we
65 extracted the longest river channel that extends from drainage divide to river mouth. Additionally, we measured parameters for each drainage system, including stream order, the length, width, aspect ratio, slope, and elevation of basins, and the length and sinuosity of rivers. The spatial distribution of drainage systems and their morphological parameters form an improved resolution global dataset, Basin90m.

70

2 Methodology

First, we divided the global DEM into 130 segments to accommodate the computational capabilities (Figs. 1 & 2a). Then, we selected a basin in Madagascar to demonstrate the processes of obtaining drainage basins and their longest rivers from a DEM through a series of
75 hydrological steps. These steps included calculating flow direction and accumulation for each



point within the basin. Based on flow direction and accumulation, we delineated basins and rivers of different stream orders (Fig. 2b). Once the spatial distribution of basins and rivers was obtained, we measured parameters describing the size and shape of the drainage systems (Fig. 2c). Finally, basins with over half of their area located in lakes or sandy deserts were removed (Fig. 2d).
80

Conventional GIS platforms such as QGIS and ArcGIS provide various hydrology tools, such as extracting drainage basins and river channels. However, in Basin90m, we need to process 130 DEMs and calculate some metrics, such as basin width, that are not conveniently calculated within GIS software. Therefore, we used the TopoToolbox software (Schwanghart and Scherler, 2014) to automate the extraction of drainage system and the calculation of various metrics in a single script. TopoToolbox is a Matlab toolbox for analyzing and manipulating geospatial data, supporting drainage basin delineation and topographic property calculation. All the operations described below in Sects. 2.2 to 2.6 were automated within our TopoToolbox script. The script inputs a single DEM and outputs vector files (ESRI shapefiles) for basins and rivers. Refer to Code availability for the download link of this script. Shapefile is a data format storing geographic vector data, including geometry and attributes. Parameters describing the morphology of the drainage systems are stored in the attribute table of the basin shapefile. The computation of all the 130 DEMs was carried out on the High Performance Computing platform of German Research Centre for Geosciences.
95

2.1 DEM preprocessing

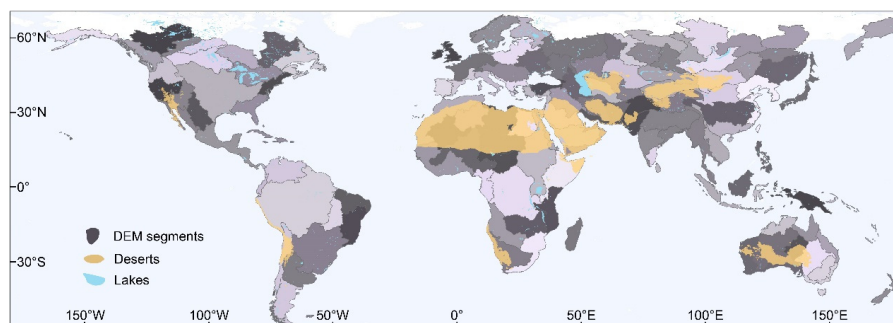
The 90-m resolution Shuttle Radar Topography Mission (SRTM) DEM is a widely used dataset for global geomorphological analyses (Farr et al., 2007). It covers the Earth's land surface between 60 degrees north and 56 degrees south latitude. Due to limitations in computer memory, it is a common practice to partition the global DEM into smaller segments, especially when working with a high-resolution global DEM (Amatulli et al., 2022). To ensure the integrity of each drainage basin and river channel, we partitioned the global DEM based on drainage divides provided by HydroBASINS (Lehner and Grill, 2013). We used the Clip Tool in ArcGIS (version 10.2) to cut the global DEM into 130 segments (Figs. 1 & 2a). By utilizing drainage divides corresponding to the largest basins in a specific region, we ensure that continents are cropped in a way that avoids splitting any basins internally. Many islands were treated as a single DEM segment, such as New Zealand (Fig. 1).
100
105

Using standard flow routing algorithms can lead to artifacts and unrealistic drainage networks, especially in lakes and deserts. Drainage systems within lakes and deserts are likely unrealistic. However, we did not remove the DEM of lakes and sandy deserts to maintain the integrity of major river basins such as the Nile River that traverses lakes and deserts. Further
110



Data description submitted to Earth System Science Data

processing of those regions was carried after obtaining the global drainage systems, as detailed in Sect. 2.7.



115 **Figure 1.** DEM segments (N=130) based on the drainage divides from HydroBASINS (Lehner and Grill, 2013). Different shades of gray are used to distinguish different DEM segments. Lakes were obtained from HydroLAKES (Messenger et al., 2016). We consider regions with an aridity index less than 0.08 as sandy desert areas (see Sect. 2.7 for detail).

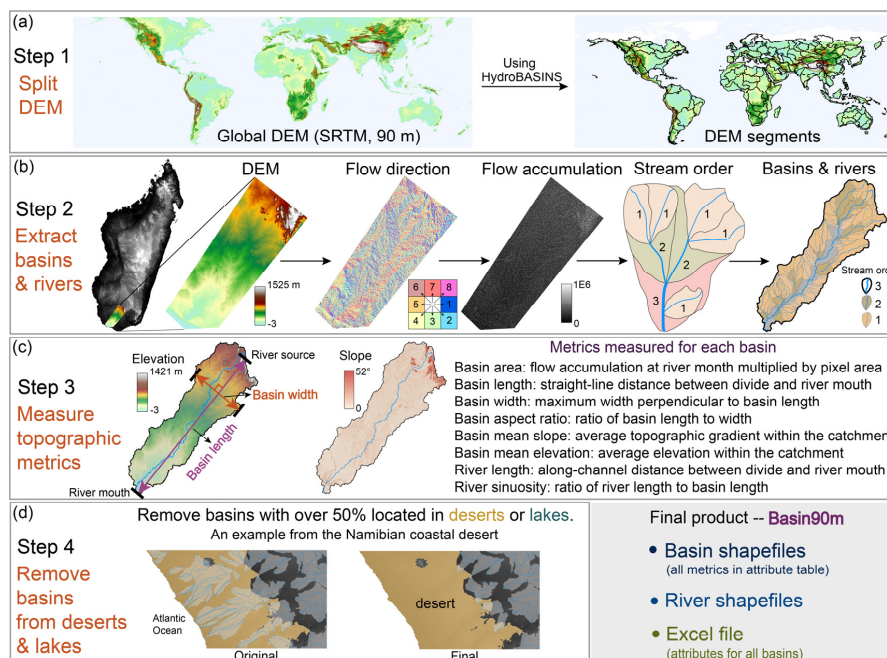
120 2.2 Flow direction

The first step to obtaining drainage basins and river networks from a DEM is to calculate flow direction and flow accumulation for all cells within the DEM. Flow direction describes the drainage direction of each cell. Flow networks derived from DEMs are affected by measurement and data processing errors (Schwanghart et al., 2013). DEM elevations in valley
125 bottoms can be overestimated due to steep hillslopes, water, and vegetation (Schwanghart and Scherler, 2017). Therefore, we used the carving method to generate flow directions to ensure channels are well connected despite local noise. Carving is a process used to remove obstacles by ensuring that, while progressing downstream, no pixel has a higher elevation than its neighboring pixels upstream (Lindsay, 2016; Schwanghart et al., 2013; Schwanghart and
130 Scherler, 2017).

Once carving is complete, we used the D8 method to determine flow direction. The D8 method is a commonly used approach for calculating river flow direction in hydrological analysis (Tarboton, 1997). The D8 method is computationally efficient and suitable for high-resolution global hydrological analysis (Lehner and Grill, 2013; Yamazaki et al., 2019; Yan et al., 2022). A single flow direction out of the eight possible directions is assigned to each cell of the DEM (Fig. 2b), by comparing the elevations of neighboring cells and identifying the steepest descent path. This method assumes that water flows directly downslope from each cell to one of its eight neighboring cells (Fig. 2b). In the D8 method, despite various ways of numbering the eight flow directions, we adopt integers from 1 to 8 to differentiate the possible
135 directions. For example, if a cell has a flow direction of 5, it indicates that all water passing through that cell will be directed towards its left neighbor (Fig. 2b). Accordingly, we used D8
140 method to calculate flow direction for all the 130 DEMs.



Data description submitted to Earth System Science Data



145 **Figure 2.** Flowchart illustrating the process of extracting the global drainage systems and their
 morphological metrics. (a) The global DEM was partitioned into 130 segments using drainage divides
 provided by HydroBASINS (Lehner et al., 2008). (b) Menarandra River Basin in southern Madagascar
 was chosen as an example to demonstrate the steps of extracting drainage basins and the longest river
 channels with various stream orders. (c) Based on the spatial distribution of basins and river channels
 150 obtained in the previous step, eight parameters describing the drainage system’s size and morphology
 were automatically measured using a Matlab script. (d) Drainage basins that have over half of their area
 within lakes or sandy deserts were removed.

2.3 Flow accumulation

155 Flow direction is the basis for calculating flow accumulation. Flow accumulation is a measure
 used in hydrological analysis to quantify the cumulative number of cells contributing to a given
 point (Fig. 2b). The flow is traced along the flow direction pathway starting from the upstream
 cells. Thus, flow accumulation starts from zero at the basin boundary, increasing downstream
 and reaching a maximum at the river mouth. The river mouth can be a location where the river
 meets a bigger river, a lake, or the ocean. Therefore, multiplying the flow accumulation of the
 160 river mouth by the pixel area of the DEM equals basin area. With flow direction and
 accumulation, we can delineate stream orders and extract basins and rivers.

2.4 Stream order

165 Large drainage basins contain small catchments. We assigned Strahler stream orders to basins
 and their longest rivers for hierarchical classification to capture this topological relationship
 between catchments. Strahler stream order is a method used to classify and quantify the



Data description submitted to Earth System Science Data

170 hierarchy of river segments within a river network (Strahler, 1957). It assigns a numerical value to each segment based on the contributing tributaries (Fig. 2b). When two segments of the same order converge, they merge to form a new segment with an order one higher. If two segments of different orders merge, the resulting segment inherits the higher order. For example, a first-order segment merging with a second-order segment results in a second-order segment. First-order rivers are often found near the basin boundary. Stream order gradually increases downstream.

175 It is important to note that the magnitude of stream order within a drainage basin depends on the area threshold of the first-order basin. The larger the threshold, the fewer orders in the entire catchment. Limited by computing resources, we only extracted and analyzed drainage basins with an area greater than or equal to 50 km². A drainage basin with an area of 50 km² contains about 6000 elevation points, sufficient to organize a drainage system. In Basin90m, basins with an area of less than 50 km² were not extracted, thus not contributing to the stream order of its downstream basins.

180

2.5 Drainage basins and the longest rivers

In TopoToolbox, basins and rivers are derived based on flow direction and accumulation. We extracted only the longest river of each basin (Fig. 2b). In natural landscapes, rivers commonly begin to develop downstream of the drainage divide by a certain distance, known as hillslope length. For example, the average hillslope lengths in Taiwan and Sicily are 1556 and 1756 m, respectively (He et al., 2021a). A common approach is to designate the point where the upstream area exceeds a certain value as the river source. This value is termed as the channelization threshold. For instance, the two latest global river databases, MERIT Hydro (Lin et al., 2021) and Hydrography90m (Amatulli et al., 2022), employ channelization thresholds of 1 and 0.05 km², respectively. Because Basin90m utilizes the straight-line distance between river source and mouth as the basin length, we selected a channelization threshold of zero, indicating that the rivers in Basin90m originate from drainage divides.

185

190

We illustrate our methodology for obtaining catchments with area larger than 50 km², using Menarandra River basin located in southern Madagascar as an example (Fig. 2b,c). This drainage basin consists of three stream orders, including one order 3, ten order 2, and forty-six order 1 sub-basins. The third-order basin has an area of 8701 km² and a basin aspect ratio of 3.3. The corresponding river length and sinuosity are 295 km and 1.6, respectively.

200 2.6 Measuring morphological indices

After obtaining the basin boundary and the longest river, we measured their basic geometric parameters. For basins, the parameters include area, length, width, aspect ratio, and average



Data description submitted to Earth System Science Data

slope and elevation (Fig. 2c). For rivers, we measured along-channel length and sinuosity (Fig. 2c). All parameters were automatically computed in our TopoToolbox script. For instance, the straight-line distance between the river source (drainage divide) and river mouth of the longest channel is used to describe basin length. The sum of elevations of all pixels within a basin divided by the number of pixels yields the basin mean elevation. We report all of these eight metrics and stream order values for catchments with a size larger than 50 km². The value of these metrics is stored in the attribute table of each basin shapefile data. See data availability statement for details.

2.7 Removing basins from lakes and deserts

After obtaining the global distribution of drainage systems, we removed basins and rivers associated with lakes and sandy deserts (Fig. 2d). Basin90m aims to provide drainage systems created by surface water flow processes. While lakes are related to water flow, it is inappropriate to consider a drainage basin completely within a lake. We need a global lake database to remove drainage systems within lakes. Several global lake datasets are available, such as HydroLAKES (Messenger et al., 2016), GloLakes (Hou et al., 2022) and Lake-TopoCat (Sikder et al., 2023). Here, we used HydroLAKES, which includes 1.4 million lakes worldwide, with an area range of 0.1-377002 km². Since the minimum basin area in Basin90m is 50 km², we only retained 3402 lakes with a size greater than 50 km² (Fig. 1).

Due to high permeability and intense evaporation, sandy deserts are typically unable to sustain surface water. Therefore, basins and rivers derived from DEMs within sandy deserts are unlikely to accurately reflect river dynamics. To our knowledge, no published global dataset for sandy deserts exists. As a result, we relied on using the aridity index to determine the location of such regions. The aridity index is a measure that quantifies the dryness or aridity of a region based on the ratio of precipitation to potential evapotranspiration. A lower aridity index indicates a drier environment. Therefore, aridity index is closely associated with desert formation (Gamo et al., 2013). Here, we used the Global-AI_PET_v3 (Zomer et al., 2022), a global aridity index dataset, to delineate sandy deserts. By comparing the regions obtained using multiple aridity index thresholds with the distribution of sandy deserts on Google Earth, we classified areas with aridity index values less than 0.08 as sandy deserts. This threshold captures the majority of sandy deserts while avoiding misclassifying excessive non-desert regions.

Using the Python-based GeoPandas library, we removed basins where over half of their area is within lakes or sandy deserts (Fig. 2d). We also removed the river channels within those deleted basins. In addition to filtering basins associated with lakes and deserts, we manually removed all drainage systems intersecting with the 60°N latitude line in ArcGIS to avoid incomplete river networks due to DEM coverage. In the end, out of the 840000 basins obtained



in Sect. 2.5, approximately 170000 were removed, retaining 667629 basins and their longest
240 rivers.

3 Results and discussions

Through the steps above, we obtained the spatial distribution of global drainage systems and
their morphological metrics. Next, we analyze the distribution and correlations of these metrics
245 in Basin90m. First, we present the differences in drainage systems with different stream orders.
Then, we show the distribution of metrics that describe the morphology of the drainage systems
globally. Afterward, we present the interrelationships among these metrics. For example,
utilizing Basin90m, we derived Hack's law (Hack, 1957) fitted from global data.

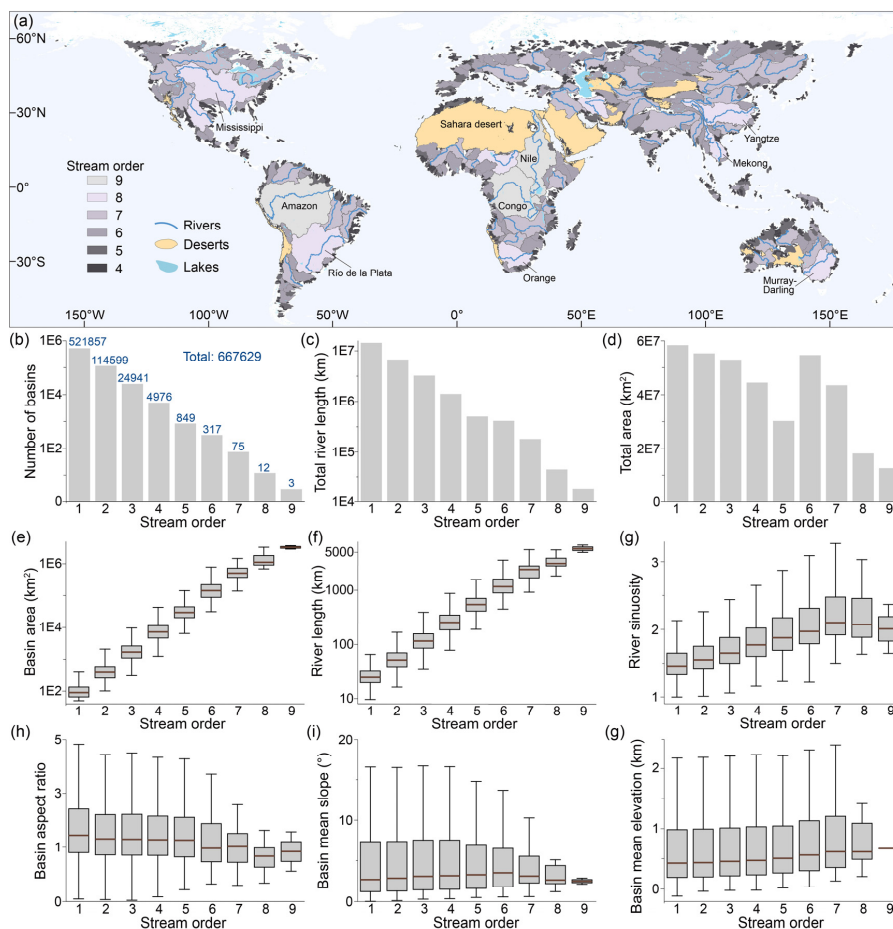
250 3.1 Basins with different stream orders

Fig. 3a shows basins in Basin90m with stream orders ranging from 4 to 9. The three ninth-order
basins are the Amazon, Nile, and Congo, with an area of 6038417, 2895947, and 3716644 km²,
respectively. Eighth-order basins are widely distributed globally, including the Mississippi in
North America, the Río de la Plata in South America, the Orange in Africa, the Yangtze and
255 Mekong in Asia, and the Murray-Darling in Australasia. Basins with the highest stream order
in a region often occupy a significant portion of the area. For example, Madagascar has a basin
with a stream order 6, covering an area of 59200 km², approximately 10% of Madagascar's
total area. Taiwan island has two basins with a stream order of 4, each with an area of about
30000 km², together occupying one-sixth of the island.

260 Fig. 3b-g illustrates the statistics of drainage systems with different stream orders. As
stream order increases, the number of basins and total river length exponentially decrease (Fig.
3b,c). The number of first-order basins is 521857, accounting for 78% of the total basin count.
There are 661397 basins with orders 1-3, representing 99% of the total basin count. In contrast,
only 90 basins are of the highest stream orders (7-9). The total basin area is determined by
265 multiplying the basin count with the average basin area. As stream order increases, the average
basin area increases while the basin count decreases. Therefore, total basin area does not
systematically change with stream order (Fig. 3d). The average basin area and river length
increase with increasing stream order because higher-order basins encompass lower-order
basins (Fig. 3e,f). River sinuosity generally increases with higher stream orders (Fig. 3g), as
270 higher-order basins provide more space for rivers to meander (Biron et al., 2014). The lack of
significant changes in basin aspect ratio with increasing stream order (Fig. 3h), along with the
absence of a correlation between basin topography (slope and elevation) and stream order (Fig.
3i,g), supports the concept of self-similarity in drainage basins (Bennett and Liu, 2016; Mantilla
et al., 2010; Sassolas-Serrayet et al., 2018).



Data description submitted to Earth System Science Data



275

Figure 3. Global drainage systems with nine stream orders. (a) The spatial distribution of basins with orders from four to nine. Rivers with stream orders from 7 to 9 are displaced. (b-g) Morphological metrics displayed by stream orders.

280 3.2 Distribution of morphological metrics

We present the probability density distributions and spatial patterns of metrics that describe the morphological characteristics of the global drainage systems. Most morphological metrics have left-skewed log-normal distributions (Fig. 4). Ninety-five percent of basins have an area smaller than 1000 km². There are only 2868 basins with a size larger than 10000 km² (Fig. 4a). Most (88%) basins have a length ranging from 10 to 50 km, with an average value of 25 km (Fig. 4b). The number of basins with lengths exceeding 100 km is 11357, accounting for only 1.7%. The average basin length is roughly twice the average basin width. Many basins (N = 89673) have an average width ranging from 5 to 25 km, constituting 87% of the total (Fig. 4c). The number of basins with aspect ratio between one and five is 598426, accounting for 90% of all basins (Fig. 4d). A basin aspect ratio less than one typically indicates a significant deviation between

285

290



Data description submitted to Earth System Science Data

the overall flow direction and the elongation direction of the basin. These are only 5% of the basins ($N = 34357$), suggesting that a deviation between the elongation and flow direction in river basins is rare.

The average slope shows a wider distribution compared to the other parameters. It is distributed between 0 and 40°, with an average value of 5.4° (Fig. 4e). Basin mean elevation directly reflects the distribution of elevations globally with multiple peaks. Among them, the peak at an elevation of 4500 m corresponds to the Tibetan Plateau and Andes (Fig. 4f). Over 95% of the river lengths are smaller than 100 km (Fig. 4g). The number of basins with river lengths exceeding 100 km and 1000 km is 31392 and 370, respectively. Since river sinuosity is the ratio between the along-channel length and the straight-line distance from the source to the mouth of a river, the minimum value is one. Basins with a river sinuosity less than two account for 91%, with an average value of 1.6 (Fig. 4h).

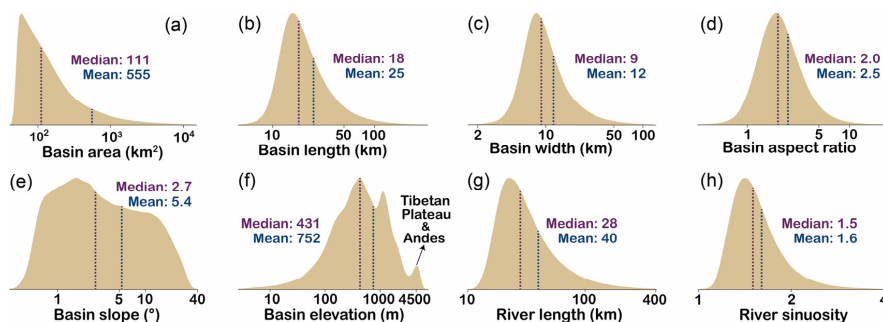


Figure 4. The probability density estimation shows the distribution of morphological metrics. All basins in Basin90m were used for probability density estimation without distinguishing stream orders. The X-axis of all subfigures is logarithmically scaled with a base of ten. (a) Basin area. (b) Basin length. (c) Basin width. (d) Basin aspect ratio. (e) Basin mean topographic slope. (f) Basin mean elevation. (g) The length of the longest river channels. (h) The sinuosity of the longest river channels. Purple and blue dashed lines indicate the median and the mean, respectively.

Basin90m includes eight metrics for each drainage system (Figs. 2c & 4). Here, we present the spatial distribution of four of them (Fig. 5). The first parameter is drainage area, which describes basin size. There are 12 basins with an area larger than 1 million km², with stream orders ranging from 7 to 9 (Fig. 5a). The second parameter is aspect ratio, illustrating basin shape. A higher aspect ratio indicates a more elongated basin. There is no clear relationship between aspect ratio and stream order (Fig. 3h). As a result, the most elongated basins can be both large and small (Fig. 5b). Numerous elongated basins characterize the Tibetan Plateau and its surrounding areas. An aspect ratio smaller than one indicates that the overall flow direction of the river is not aligned with the elongation direction of the basin. For example, the Congo River flows from west to east, while the longest direction of the basin is north-south. This results in an aspect ratio of 0.9 for the Congo Basin.

The third metric is the average slope of the basin, demonstrating the topographic variations

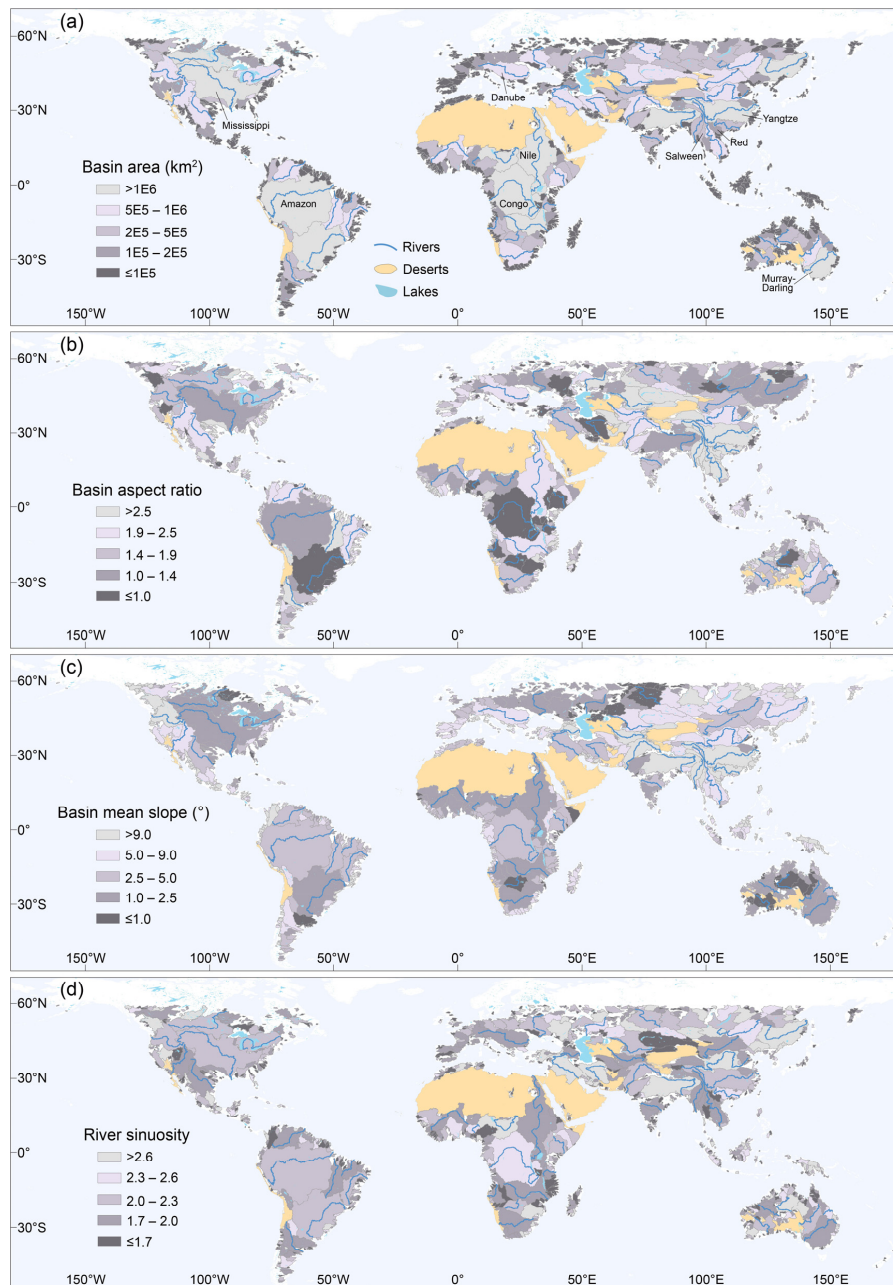


Data description submitted to Earth System Science Data

within the catchment. Due to the significant elevation differences between the Tibetan Plateau and the surrounding plains, steep basins have developed around the plateau (Fig. 5c). The
325 average slopes of the Yangtze, Salween, and Red Basins around the plateau margin are 13, 17,
and 18°, respectively. In contrast, the slopes of the Murray-Darling, Mississippi, and Amazon
basins are only 1, 2, and 3°, respectively. The fourth parameter is river sinuosity, describing the
shape of the longest river. A high sinuosity indicates a meandering river, while a sinuosity closer
to one indicates a straight river. The sinuosity of the Nile, Danube, Amazon, and Mississippi
330 rivers are 1.6, 1.8, 2, and 2.3, respectively (Fig. 5d).



Data description submitted to Earth System Science Data



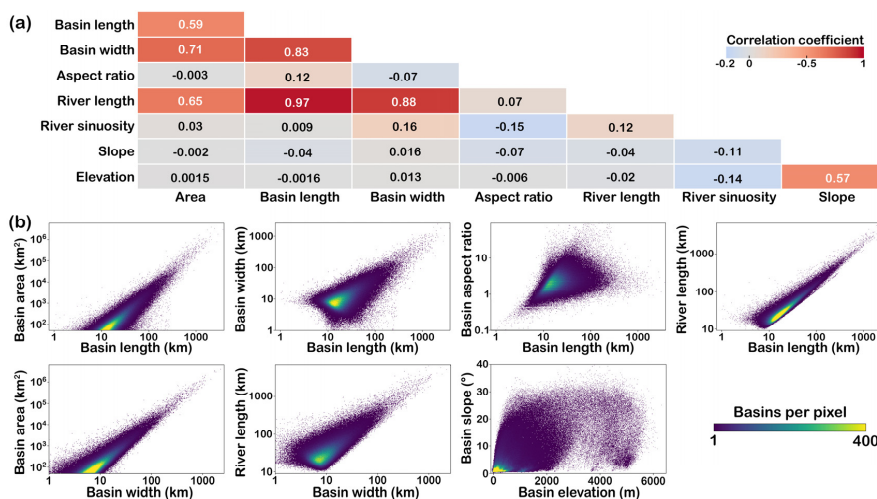
335 **Figure 5.** The global distribution of drainage systems with various metrics. Note that higher-order basins cover the lower-order basins. Drainage basins colored by basin area (a), basin aspect ratio (b), basin mean topographic slope (c), and river sinuosity (d). Rivers (blue) with stream orders from 7 to 9 are displaced.



340 3.3 Relationship between morphological metrics

The eight metrics in Basin90m describe the size and shape of drainage systems from various perspectives. The correlation among these parameters is crucial for understanding landscape dynamics, thus we present a visualization of their relationships (Fig. 6). Overall, there is a strong correlation among parameters that describe similar features (Fig. 6a). For instance, the correlation coefficient between basin length and river length is 0.97, suggesting that river channels and basins tend to grow or shrink simultaneously. The expansion and contraction of basins are achieved through drainage divide migration, which redistributes the lengths of river channels on both sides of the drainage divide (Habousha et al., 2023; He et al., 2021b). Conversely, parameters describing different features typically exhibit a weak correlation. For example, the correlation coefficient between the area representing basin size, and the slope describing topography, is approximately zero (Fig. 6a).

Fig. 6b displays 2D density plots of correlated parameters. For example, basin area increases with increasing basin length and width. This result is expected since basins often become wider as they grow in length (correlation coefficient of 0.83, Fig. 6a), and both length and width are important factors determining area. Another example is the relatively high correlation between elevation and slope, which indicates that basins with steeper slopes tend to develop at higher elevations. It is important to note that the correlations shown in Fig. 6 represent the overall trend, with numerous exceptions exist. For instance, high-altitude plateaus have low slopes, while areas with only a few hundred meters can exhibit high slopes due to deep-cut gorges.



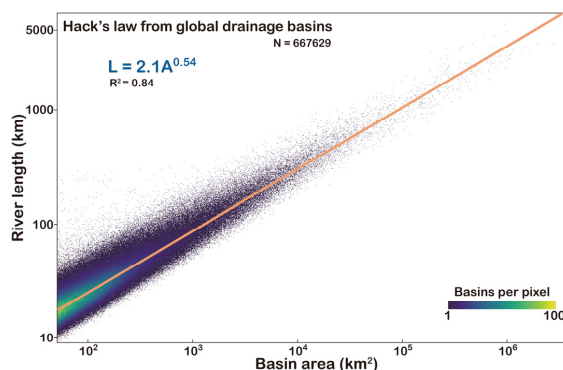
365 **Figure 6.** The correlation among metrics. (a) The table shows the linear correlation coefficients among eight metrics, highlighted by the heatmap. The correlation coefficient indicates the extent and direction of the linear relationship between two variables. It ranges from -1 to 1, where positive values signify a positive correlation, with a higher absolute value indicating a stronger relationship. (b) 2D density plot revealing relationships between selected metrics.



Data description submitted to Earth System Science Data

3.4 Hack's law

Hack's law is an empirical relationship that relates river length to basin area (Hack, 1957). It can be expressed as $L = kA^h$, where L represents the length of the longest river measured from drainage divide to river mouth, A is drainage area, k and h are constant and exponent, respectively. Hack's law is a fundamental concept in geomorphology and hydrology, and is crucial for understanding the dynamics of river networks. In addition, Hack's law derived from Earth can potentially be compared to valley systems on Mars, providing insights into its climates and hydrological processes (Luo et al., 2023; Penido et al., 2013; Som et al., 2009). Previous studies have obtained different values for k and h in Hack's law, which vary across regions. The k ranges from one to five, while the range for the h is typically 0.4-0.7 (Hack, 1957; Luo et al., 2023; Mueller, 1972; O'Malley, 2020; Sassolas-Serrayet et al., 2018; Yi et al., 2018). Recently, based on 3685 catchments globally, Hack's law with an exponent of 0.56 was obtained (O'Malley, 2020). Here, we utilized the basin areas and river lengths in Basin90m to establish a new global Hack's law with $k = 2.1 \text{ km}^{-0.08}$ and $h = 0.54$ (Fig. 7). These values not only match regional case studies (Hack, 1957; He et al., 2021a; Montgomery and Dietrich, 1992; Sassolas-Serrayet et al., 2018; Yi et al., 2018; Yuan et al., 2023), but also align with earlier results derived from global drainage systems (O'Malley, 2020).



385 **Figure 7.** Hack's law fitted based on the basin area (A) and river length (L). We used all basins in Basin90m to fit Hack's law, including all stream orders.

4 Validations and limitations

Due to the absence of a published database for a direct comparison with the eight parameters contained in Basin90m, we used the Hydrology Tool in ArcGIS (version 10.2) to extract the drainage divide and main channel of the Moche Basin in Peru. Here, we used the same DEM as Basin90m, which is the 90-m resolution SRTM DEM (Farr et al., 2007). On this foundation, we validated the accuracy of the spatial position of basin boundaries and the longest river channel against HydroSHEDS (Lehner and Grill, 2013), the drainage system extracted by ArcGIS, and the Google Earth images. We then compared the morphological metrics in



Data description submitted to Earth System Science Data

Basin90m against HydroATLAS and the measurements from ArcGIS. In addition, we discussed the limitations of Basin90m.

4.1 Spatial accuracy of drainage system

400 The accuracy of basin boundaries and river channels directly affects the calculation of the sizes and shapes of drainage systems. We used the Moche River basin in Peru as an example to verify the spatial accuracy of Basin90m, because it contains diverse terrain features (Fig. 8a). Additionally, the presence of the Moche Civilization in the downstream plain of the Moche River indicates that human modification on the landscape has been ongoing for approximately
405 three thousand years (Toyne et al., 2014). The Moche River originates in the Andes and flows into the Pacific Ocean. Nearly half of the drainage basin is located in the upstream low-relief plateau. The middle reaches consist of a deep canyon that occupies 40% of the area. The downstream area is a flat plain covering 10% of the drainage basin, and the river only decreases in elevation by 150 m over 20 km.

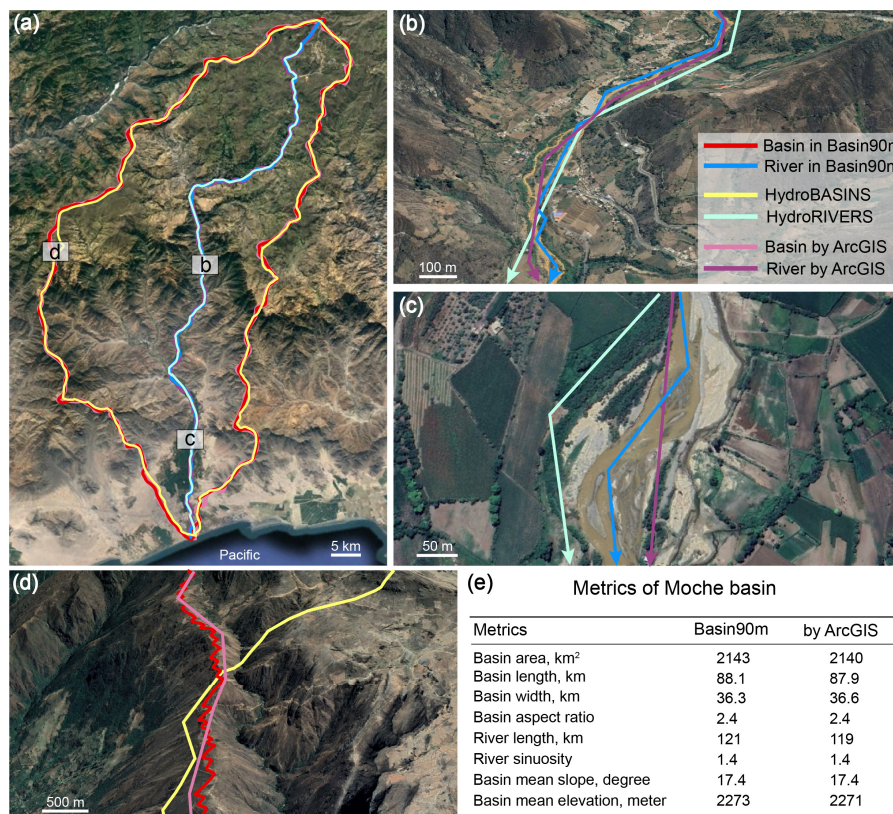
410 We compared the spatial accuracy of drainage systems in Basin90m with two datasets. The first one is HydroSHEDS which consists of HydroRIVERS and HydroBASINS (Lehner and Grill, 2013). HydroSHEDS has a spatial resolution of 500 m and has been widely used in various fields such as geomorphology, hydrology, ecology, climatology, and geohazards (McEwan et al., 2023; Palmer et al., 2023; Tu et al., 2023). The second dataset we compare
415 with Basin90m is the drainage system of Moche basin we extracted from ArcGIS using the same 90-m DEM (Farr et al., 2007). Due to the different DEM resolutions and methods in the three data, the basins and rivers only partially overlap (Fig. 8a).

In the deep canyon area (Fig. 8b), HydroRIVERS is coarse and does not match the river channel. In comparison, although Basin90m does not fully align with the real river channel,
420 there is a noticeable improvement in accuracy. The accuracy of the river extracted using ArcGIS falls between Basin90m and HydroRIVERS. The differences between the three are more pronounced in the flat plain of the downstream area (Fig. 8c). HydroRIVERS lies along the floodplain rather than the river channel. In contrast, even in such a low-relief area with human modifications, Basin90m follows the position of the river channel. Again, the performance of
425 the river obtained using ArcGIS falls between the two datasets.

We selected a segment of the drainage divide to compare the accuracy of basin boundary (Fig. 8d). The drainage divide in Basin90m follows the ridge. However, HydroBASINS does not follow the ridge and even cuts through a deeply incised river channel. Although the drainage divide extracted using ArcGIS generally follows the ridge with some degree of accuracy, it is
430 not as accurate as Basin90m. In summary, in the Moche basin, Basin90m exhibits a higher spatial accuracy than HydroSHEDS and drainage systems extracted using ArcGIS.



Data description submitted to Earth System Science Data



435 **Figure 8.** The spatial accuracy of the drainage system in Basin90m, compared against HydroSHEDS (Lehner and Grill, 2013), drainage system extracted by ArcGIS, and © Google Earth images. The Moche basin in Peru serves as an example that combines a low-relief plateau, deep canyons, and farming land in plains, simultaneously. (a) The drainage system of the Moche basin. A comparison between river channels in deep canyon region (b) and flat region (c). (d) A comparison between drainage divides. (e) A comparison of the metrics for Moche Basin between Basin90m and those extracted by ArcGIS.

440

4.2 Accuracy of morphological metrics

The morphological metrics that can be directly compared between the published databases and Basin90m only include basin area, slope, and elevation. For example, in HydroATLAS (Linke et al., 2019), the area, slope, and elevation of the Moche Basin are 2125 km², 2267 m, and 17°, respectively. This means the difference between Basin90m and HydroATLAS in Moche Basin is less than 1%. To validate the accuracy of the remaining five parameters included in Basin90m, we used the results of the Moche Basin extracted by ArcGIS. The primary difference in the extraction of drainage system between ArcGIS and our TopoToolbox script is in handling local minimum. ArcGIS uses the filling method, which completely fills depressions. In TopoToolbox, we used the carving method, which carves a channel through local depressions to allow the

445
450



Data description submitted to Earth System Science Data

river to flow out. Therefore, although both used the same DEM, there are still slight differences in the positions of drainage system (Fig. 8a-d). Except for a 1.6% difference in river length, all the remaining seven parameters exhibit variances of less than 0.8%. Basin90m's river channels and drainage divides are more detailed than those extracted by ArcGIS (Fig. 8b-d), resulting in longer river channels. Therefore, Basin90m has higher spatial accuracy (Fig. 8b-d) and provides more accurate values for the morphometric metrics (Fig. 8e).

4.3 Limitations

Although Basin90m has improved the spatial accuracy of drainage systems compared to HydroSHEDS, it still has some limitations. First, the basins and rivers in Basin90m are entirely based on DEM analysis. Therefore, the measurement and processing errors of the DEM itself can affect the spatial accuracy of Basin90m. Second, in nature, rivers can flow in any direction. But the D8 method was used to calculate flow direction, which reduces computational complexity but limits the flow to only eight directions. Third, after obtaining 667629 global basins and their longest rivers, no manual removal of false rivers has been conducted, especially in flat areas. Users must consider these limitations when using and interpreting the results of Basin90m, particularly in flat regions and in areas with severe human modifications.

5 Data availability

Basin90m is freely available at <https://dataservices.gfz-potsdam.de/panmetaworks/review/218da89b6b9388ce9161dc8462bd0ad65904300f2ec0fecfb53b45788c5614aa/> (He et al., 2023). Basin90m contains 667629 drainage basins with areas larger than 50 km². Each basin is accompanied by its longest river channel, from drainage divide to river mouth. Basins and rivers are stored in ESRI shapefile format, which can be opened and edited using GIS software (e.g., QGIS and ArcGIS) and Python libraries (e.g., GeoPandas). The data is grouped by six continents. Each continent contains multiple stream orders. For example, the basin files for Europe consist of eight shapefiles corresponding to stream orders 1-8. The filenames of basins and rivers include the stream order and continent information. For instance, "Africa_Basin_5.shp" contains all African basins with a stream order of 5. The eight parameters (Fig. 2c) describing the size and shape of drainage systems were stored in the attribute tables of the basin shapefiles. The shapefiles for global basins and rivers are 7.8 and 2.5 GB, respectively. The attribute tables of all global basins were merged into a single Excel file (Basin90m.xlsx).

485



Data description submitted to Earth System Science Data

6 Code availability

The Matlab script (Basin90m.m) used to generate Basin90m and a user guide are freely available at <https://dataservices.gfz-potsdam.de/panmetaworks/review/218da89b6b9388ce9161dc8462bd0ad65904300f2ec0fecfb53b45788c5614aa/>. Note that before running this code, one needs to install TopoToolbox (Schwanghart and Scherler, 2014). The link <https://topotoolbox.wordpress.com/topotoolbox/> provides installation and usage instructions for TopoToolbox.

7 Conclusions

Here we present Basin90m, a global dataset of the shape of drainage systems. Utilizing a 90-m resolution DEM, we extracted 667629 drainage basins with an area larger than 50 km². Each basin contains only one longest river channel, extending from the upstream drainage divide to the downstream river mouth. Basin90m provides information on the size, shape, hierarchy, and topography of drainage basins, as well as the length and sinuosity of river channels. Compared to the published datasets, Basin90m offers a higher resolution, includes the shape of basins and rivers, and excludes drainage systems with over half of their area located in lakes and sandy deserts.

First, we presented the variations among different stream orders regarding quantity, size, and shape of drainage systems. The number of basins decreased from 521857 for the first order to 3 for the ninth order. In contrast, increasing stream order increased the average basin area, river length, and sinuosity. Second, we displayed the probability and spatial distribution of the eight parameters. The most notable feature is that numerous narrow and steep basins are distributed in the margins of the Tibetan Plateau. We then demonstrated the correlations among the eight parameters. The highest correlation coefficient of 0.97 was found between basin length and river length, indicating the coevolution of rivers and basins in nature. Using the basin area and river length from Basin90m, we fitted a global Hack's law as $L=2.1A^{0.54}$.

To validate the accuracy of Basin90m, we compared it with multiple data sources using the Moche Basin in Peru as an example. This comparison included HydroSHEDS for river and basin boundaries, Google Earth images, drainage systems extracted using ArcGIS, and HydroATLAS for basin area, elevation, and slope. The results showed that Basin90m exhibited the highest spatial accuracy. Furthermore, the difference between morphological parameters in Basin90m and other data sources is typically less than 1%. These validations confirm the reliability and accuracy of Basin90m as a valuable resource for studying and analyzing drainage systems on a global scale.



Data description submitted to Earth System Science Data

Author contributions

CH, CJY, and JMT conceived the initial idea. CH performed calculations and data processing,
525 wrote a first draft, and made the figures. CJY built the code to extract Basin90m from DEM,
with inputs from RFO. JMT designed method for measuring the length and width of drainage
basin. RFO collected the global DEM. GSdQ proposed using the aridity index to automatically
classify sandy deserts. JB, HT, SG, and XPY participated in data processing and analysis. All
authors contributed to the conceptualization, discussion, data collection, and editing of all
530 components of Basin90m and this manuscript.

Competing interests

The contact author has declared that none of the authors has any competing interests.

535 Acknowledgements

We appreciate the High Performance Computing team at German Research Centre for
Geosciences (GFZ) for their technical support during our calculations. We thank Kirsten Elger
from the GFZ Library and Information Services for the help in uploading and managing
Basin90m data in GFZ Data Services. We thank Gareth Roberts and Jingtao Lai for discussions.

540

Financial support

CH acknowledges support from NSFC (National Natural Science Foundation of China) (Grant
42201008) and Helmholtz-OCPC Postdoc Program (No. 202120). XPY acknowledges funding
from NSFC (Grant 42272261).

545 References

- Allen, G. H. and Pavelsky, T. M.: Global extent of rivers and streams, *Science*, 361, 585–588,
<https://doi.org/10.1126/science.aat0636>, 2018.
- Amatulli, G., Marquez, J. G., Sethi, T., Kiesel, J., Grigoropoulou, A., Üblacker, M. M., Shen, L. Q., and
Domisch, S.: Hydrography90m: a new high-resolution global hydrographic dataset, *Earth Syst. Sci.*
550 *Data*, 14, 4525–4550, <https://doi.org/10.5194/essd-14-4525-2022>, 2022.
- Bennett, S. J. and Liu, R.: Basin self-similarity, Hack's law, and the evolution of experimental rill
networks, *Geology*, 44, 35–38, <https://doi.org/10.1130/G37214.1>, 2016.
- Biron, P. M., Buffin-Belanger, T., Larocque, M., Chone, G., Cloutier, C. A., Ouellet, M. A., Demers, S.,
Olsen, T., Desjarlais, C., and Eyquem, J.: Freedom space for rivers: a sustainable management
555 approach to enhance river resilience, *Environ. Manage.*, 54, 1056–1073,
<https://doi.org/10.1007/s00267-014-0366-z>, 2014.
- Castelltort, S., Goren, L., Willett, S. D., Champagnac, J.-D., Herman, F., and Braun, J.: River drainage
patterns in the New Zealand Alps primarily controlled by plate tectonic strain, *Nat. Geosci.*, 5, 744–
748, <https://doi.org/10.1038/ngeo1582>, 2012.
- 560 Farr, T. G., Rosen, P. A., Caro, E., Crippen, R., Duren, R., Hensley, S., Kobrick, M., Paller, M., Rodriguez,



Data description submitted to Earth System Science Data

- E., Roth, L., Seal, D., Shaffer, S., Shimada, J., Umland, J., Werner, M., Oskin, M., Burbank, D., and Alsdorf, D.: The Shuttle Radar Topography Mission, *Rev. Geophys.*, 45, RG2004, <https://doi.org/10.1029/2005RG000183>, 2007.
- 565 Gamo, M., Shinoda, M., and Maeda, T.: Classification of arid lands, including soil degradation and irrigated areas, based on vegetation and aridity indices, *Int. J. Remote Sens.*, 34, 6701-6722, <https://doi.org/10.1080/01431161.2013.805281>, 2013.
- Guth, P. L.: Drainage basin morphometry: a global snapshot from the shuttle radar topography mission, *Hydrol. Earth Syst. Sci.*, 15, 2091-2099, <https://doi.org/10.5194/hess-15-2091-2011>, 2011.
- 570 Habousha, K., Goren, L., Nativ, R., and Gruber, C.: Plan-form evolution of drainage basins in response to tectonic changes: Insights from experimental and numerical landscapes, *J. Geophys. Res.: Earth Surf.*, 128, e2022JF006876, <https://doi.org/10.1029/2022JF006876>, 2023.
- Hack, J. T.: Studies of longitudinal stream profiles in Virginia and Maryland, United States Geological Survey, <https://pubs.usgs.gov/pp/0294b/report.pdf>, 1957.
- 575 He, C., Yang, C. J., Turowski, J. M., Rao, G., Roda-Boluda, D. C., and Yuan, X. P.: Constraining tectonic uplift and advection from the main drainage divide of a mountain belt, *Nat. Commun.*, 12, 544, <https://doi.org/10.1038/s41467-020-20748-2>, 2021a.
- He, C., Yang, C. J., Rao, G., Roda-Boluda, D. C., Yuan, X. P., Yang, R., Gao, L., and Zhang, L.: Landscape response to normal fault linkage: Insights from numerical modeling, *Geomorphology*, 388, 107796, <https://doi.org/10.1016/j.geomorph.2021.107796>, 2021b.
- 580 He, C., Yang, C. J., Turowski, J. M., Ott, R. F., Braun, J., Tang, H., Ghantous, S., Yuan, X. P., Stucky de Quay, G.: Basin90m, a new global drainage basin dataset. GFZ Data Services, <https://doi.org/10.5880/GFZ.4.6.2023.004>, 2023.
- Hou, J., Van Dijk, A. I. J. M., Renzullo, L. J., and Larraondo, P. R.: GloLakes: a database of global lake water storage dynamics from 1984 to present derived using laser and radar altimetry and optical remote sensing, *Earth Syst. Sci. Data*, <https://doi.org/10.5194/essd-2022-266>, 2022.
- 585 Ielpi, A., Lapôtre, M. G. A., Finotello, A., and Roy-Léveillé, P.: Large sinuous rivers are slowing down in a warming Arctic, *Nat. Clim. Change*, 13, 375-381, <https://doi.org/10.1038/s41558-023-01620-9>, 2023.
- Lehner, B. and Grill, G.: Global river hydrography and network routing: baseline data and new approaches to study the world's large river systems, *Hydrol. Processes*, 27, 2171-2186, <https://doi.org/10.1002/hyp.9740>, 2013.
- 590 Lehner, B., Verdin, K., and Jarvis, A.: New global hydrography derived from spaceborne elevation data, *Eos, Trans., Am. Geophys. Union*, 89, 93-104, <https://doi.org/10.1029/2008EO100001>, 2008.
- Lin, P., Pan, M., Wood, E. F., Yamazaki, D., and Allen, G. H.: A new vector-based global river network dataset accounting for variable drainage density, *Sci. Data*, 8, 28, <https://doi.org/10.1038/s41597-021-00819-9>, 2021.
- 595 Lindsay, J. B.: Efficient hybrid breaching-filling sink removal methods for flow path enforcement in digital elevation models, *Hydrol. Processes*, 30, 846-857, <https://doi.org/10.1002/hyp.10648>, 2016.
- 600 Linke, S., Lehner, B., Ouellet Dallaire, C., Ariwi, J., Grill, G., Anand, M., Beames, P., Burchard-Levine, V., Maxwell, S., Moidu, H., Tan, F., and Thieme, M.: Global hydro-environmental sub-basin and river reach characteristics at high spatial resolution, *Sci. Data*, 6, 283, <https://doi.org/10.1038/s41597-019-0300-6>, 2019.
- Luo, W., Howard, A. D., Craddock, R. A., Oliveira, E. A., and Pires, R. S.: Global spatial distribution of Hack's Law exponent on Mars consistent with early arid climate, *Geophys. Res. Lett.*, 50,



Data description submitted to Earth System Science Data

- 605 e2022GL102604, <https://doi.org/10.1029/2022GL102604>, 2023.
- Mantilla, R., Troutman, B. M., and Gupta, V. K.: Testing statistical self-similarity in the topology of river networks, *J. Geophys. Res.*, 115, F03038, <https://doi.org/10.1029/2009JF001609>, 2010.
- Masutomi, Y., Inui, Y., Takahashi, K., and Matsuoka, Y.: Development of highly accurate global polygonal drainage basin data, *Hydrol. Processes*, 23, 572-584, <https://doi.org/10.1002/hyp.7186>, 2009.
- 610 McEwan, E., Stahl, T., Howell, A., Langridge, R., and Wilson, M.: Coseismic river avulsion on surface rupturing faults: Assessing earthquake-induced flood hazard, *Science*, 9, eadd2932, <https://doi.org/10.1126/sciadv.add293>, 2023.
- Messenger, M. L., Lehner, B., Grill, G., Nedeva, I., and Schmitt, O.: Estimating the volume and age of water stored in global lakes using a geo-statistical approach, *Nat. Commun.*, 7, 13603, <https://doi.org/10.1038/ncomms13603>, 2016.
- 615 Montgomery, D. R. and Dietrich, W. E.: Channel initiation and the problem of landscape scale, *Science*, 255, 826-830, <https://doi.org/10.1126/science.255.5046.826>, 1992.
- Mueller, J. E.: Re-evaluation of the relationship of master streams and drainage basins, *Geol. Soc. Am. Bull.*, 83, 3471-3474, [https://doi.org/10.1130/0016-7606\(1972\)83\[3471:ROTTROM\]2.0.CO;2](https://doi.org/10.1130/0016-7606(1972)83[3471:ROTTROM]2.0.CO;2), 1972.
- 620 Nagayama, S. and Nakamura, F.: The significance of meandering channel to habitat diversity and fish assemblage: a case study in the Shibetsu River, northern Japan, *Limnology*, 19, 7-20, <https://doi.org/10.1007/s10201-017-0512-4>, 2017.
- O'Malley, C. P. B.: Quantitative analysis of river profiles and fluvial landscapes, Doctoral dissertation, University of Cambridge, <https://doi.org/10.17863/CAM.51663>, 2020.
- 625 Palmer, P. I., Wainwright, C. M., Dong, B., Maidment, R. I., Wheeler, K. G., Gedney, N., Hickman, J. E., Madani, N., Folwell, S. S., Abdo, G., Allan, R. P., Black, E. C. L., Feng, L., Gudoshava, M., Haines, K., Huntingford, C., Kilavi, M., Lunt, M. F., Shaaban, A., and Turner, A. G.: Drivers and impacts of Eastern African rainfall variability, *Nat. Rev. Earth Environ.*, 4, 254-270, <https://doi.org/10.1038/s43017-023-00397-x>, 2023.
- 630 Penido, J. C., Fassett, C. I., and Som, S. M.: Scaling relationships and concavity of small valley networks on Mars, *Planet. Space Sci.*, 75, 105-116, <https://doi.org/10.1016/j.pss.2012.09.009>, 2013.
- Rhoads, B. L., Schwartz, J. S., and Porter, S.: Stream geomorphology, bank vegetation, and three-dimensional habitat hydraulics for fish in midwestern agricultural streams, *Water Resour. Res.*, 39, 1218, <https://doi.org/10.1029/2003WR002294>, 2003.
- 635 Sassolas-Serrayet, T., Cattin, R., and Ferry, M.: The shape of watersheds, *Nat. Commun.*, 9, 3791, <https://doi.org/10.1038/s41467-018-06210-4>, 2018.
- Schwanghart, W., Groom, G., Kuhn, N. J., and Heckrath, G.: Flow network derivation from a high resolution DEM in a low relief, agrarian landscape, *Earth Surf. Process. Landf.*, 38, 1576-1586, <https://doi.org/10.1002/esp.3452>, 2013.
- 640 Schwanghart, W. and Scherler, D.: Bumps in river profiles: uncertainty assessment and smoothing using quantile regression techniques, *Earth Surf. Dyn.*, 5, 821-839, <https://doi.org/10.5194/esurf-5-821-2017>, 2017.
- Schwanghart, W. and Scherler, D.: Short communication: TopoToolbox 2 – MATLAB-based software for topographic analysis and modeling in Earth surface sciences, *Earth Surf. Dyn.*, 2, 1-7, <https://doi.org/10.5194/esurf-2-1-2014>, 2014.
- 645 Shen, X., Anagnostou, E. N., Mei, Y., and Hong, Y.: A global distributed basin morphometric dataset, *Sci. Data*, 4, 160124, <https://doi.org/10.1038/sdata.2016.124>, 2017.



Data description submitted to Earth System Science Data

- 650 Sikder, M. S., Wang, J., Allen, G. H., Sheng, Y., Yamazaki, D., Song, C., Ding, M., Crétaux, J.-F., and Pavelsky, T. M.: Lake-TopoCat: A global lake drainage topology and catchment database, *Earth Syst. Sci. Data*, 15, 3483-3511, <https://doi.org/10.5194/essd-15-3483-2023>, 2023.
- Som, S. M., Montgomery, D. R., and Greenberg, H. M.: Scaling relations for large Martian valleys, *J. Geophys. Res.*, 114, E02005, <https://doi.org/10.1029/2008JE003132>, 2009.
- 655 Sreedevi, P. D., Owais, S., Khan, H. H., and Ahmed, S.: Morphometric analysis of a watershed of South India using SRTM data and GIS, *J. Geol. Soc. India*, 73, 543-552, <https://doi.org/10.1007/s12594-009-0038-4>, 2009.
- Strahler, A. N.: Quantitative analysis of watershed geomorphology, *Eos, Trans., Am. Geophys. Union*, 38, 913-920, <https://doi.org/10.1029/TR038i006p00913>, 1957.
- 660 Strong, C. M. and Mudd, S. M.: Explaining the climate sensitivity of junction geometry in global river networks, *PNAS*, 119, e2211942119, <https://doi.org/10.1073/pnas.2211942119>, 2022.
- Tarboton, D. G.: A new method for the determination of flow directions and upslope areas in grid digital elevation models, *Water Resour. Res.*, 33, 309-319, <https://doi.org/10.1029/96WR03137>, 1997.
- Toyne, J. M., White, C. D., Verano, J. W., Uceda Castillo, S., Millaire, J. F., and Longstaffe, F. J.: Residential histories of elites and sacrificial victims at Huacas de Moche, Peru, as reconstructed from oxygen isotopes, *J. Archaeol. Sci.*, 42, 15-28, <https://doi.org/10.1016/j.jas.2013.10.036>, 2014.
- 665 Tu, T., Comte, L., and Ruhi, A.: The color of environmental noise in river networks, *Nat. Commun.*, 14, 1728, <https://doi.org/10.1038/s41467-023-37062-2>, 2023.
- USGS: HYDRO1k elevation derivative database, U.S. Geol. Surv., <https://doi.org/10.5066/F77P8WN0>, 2000.
- 670 Verdin, K. L.: Hydrologic derivatives for modeling and applications (HDMA) database-A new global high-resolution database, U.S. Geol. Surv., Virginia, <https://doi.org/10.3133/ds1053>, 2017.
- Vörösmarty, C. J., Fekete, B. M., Meybeck, M., and Lammers, R. B.: Global system of rivers: Its role in organizing continental land mass and defining land-to-ocean linkages, *Global Biogeochem. Cycles*, 14, 599-621, <https://doi.org/10.1029/1999GB900092>, 2000.
- 675 Yamazaki, D., Ikeshima, D., Sosa, J., Bates, P. D., Allen, G. H., and Pavelsky, T. M.: MERIT Hydro: A high-resolution global hydrography map based on latest topography dataset, *Water Resour. Res.*, 55, 5053-5073, <https://doi.org/10.1029/2019WR024873>, 2019.
- Yan, D., Li, C., Zhang, X., Wang, J., Feng, J., Dong, B., Fan, J., Wang, K., Zhang, C., Wang, H., Zhang, J., and Qin, T.: A data set of global river networks and corresponding water resources zones divisions v2, *Sci. Data*, 9, 770, <https://doi.org/10.1038/s41597-019-0243-y>, 2022.
- 680 Yi, R. S., Arredondo, Á., Stansifer, E., Seybold, H., and Rothman, D. H.: Shapes of river networks, *Proc. R. Soc. A* 474, 20180081, <https://doi.org/10.1098/rspa.2018.0081>, 2018.
- Yu, Z., Zhang, J., Wang, H., Zhao, J., Dong, Z., Peng, W., and Zhao, X.: Quantitative analysis of ecological suitability and stability of meandering rivers, *Front. Biosci. Landmark*, 27, 42, <https://doi.org/10.31083/j.fbl2702042>, 2022.
- 685 Yuan, X. P., Jiao, R., Liu-Zeng, J., Dupont-Nivet, G., Wolf, S. G., Shen, X.: Downstream propagation of fluvial erosion in Eastern Tibet. *Earth Planet. Sci. Lett.*, 605, 118017, <https://doi.org/10.1016/j.epsl.2023.118017>, 2023.
- Zomer, R. J., Xu, J., and Trabucco, A.: Version 3 of the Global Aridity Index and Potential Evapotranspiration Database, *Sci. Data*, 9, 409, <https://doi.org/10.1038/s41597-022-01493-1>, 2022.
- 690